Origins of significant reduction of lattice thermal conductivity in graphene allotropes

Usama Choudhry,* Shengying Yue,* and Bolin Liao†
Department of Mechanical Engineering, University of California, Santa Barbara, California 93106, USA

(Received 16 April 2019; revised manuscript received 13 August 2019; published 1 October 2019)

Lattice dynamics in artificial periodic structures, or "phononic crystals", have attracted significant research interest, thanks to the potential to manipulate acoustic wave propagation with more flexibility. The same control on heat conduction, however, has proven challenging due to the short wavelength of thermal phonons. In this work, we use first-principles simulations to characterize the previously unstudied thermal properties of dodecagraphene and tetragraphene, two-dimensional (2D) carbon allotropes based upon graphene but containing a secondary, in-plane periodicity. Surprisingly, we find that despite very similar atomic structure and bonding strength, they possess significantly different thermal properties than that of graphene: at room temperature, their thermal conductivity is up to 80% lower than that of graphene. We attribute these distinct properties to the presence of naturally occurring, low frequency optical phonon modes that arise from a folding of the acoustic modes due to the superstructure and the associated frequency gap opening. Furthermore, we observe significantly enhanced Umklapp scatterings in both carbon allotropes that largely suppress the hydrodynamic phonon transport in pristine graphene. Our study presents dodecagraphene and tetragraphene as ideal model systems to explore lattice dynamics in 2D and demonstrates the potential to significantly modify thermal transport of 2D materials without making drastic changes to their fundamental compositions.

DOI: 10.1103/PhysRevB.100.165401

I. INTRODUCTION

The *in situ* control of wave propagation through conventional media is of great interest and significance to many problems across numerous fields. Significant research has been put into the design and engineering of metamaterials, artificial structures that typically have periodic orders matching the wavelength of the propagating waves (e.g., light and sound), resulting in highly unusual bulk material properties that are typically not found naturally. Photonic metamaterials, or photonic crystals, have provided unprecedented capability to control the propagation of light [1]. Acoustic metamaterials have been designed with negative indices of refraction [2] or negative bulk moduli [3], for uses in applications such as acoustic cloaking or acoustic imaging. Successful manipulation of wave propagation in materials typically requires a feature size comparable to or smaller than the relevant wavelengths present. This makes the design of effective thermal metamaterials difficult, as the wavelength of thermally relevant phonons is typically on the order of a few nanometers. Creating "phononic crystals" for thermal phonons holds the promise of transformative opportunities in thermal transport control [4–7], but remains largely unexplored due to the small wavelength of thermal phonons. Luckyanova *et al.* observed enhanced thermal conductivity in GaAs/AlAs superlattices [8] with a 24-nm period due to coherent transport of long wavelength acoustic phonons across the interfaces, and further discovered coherent backscattering, or localization, of phonons in the same structure [9] with ErAs dots randomly distributed at the interfaces. Ravichandran *et al.* observed a transition from incoherent phonon scattering at interfaces to coherent phonon transport in epitaxially grown $SrTiO_3/CaTiO_3$ and $SrTiO_3/BaTiO_3$ oxide superlattices [10] when the period of the superlattices becomes approximately 1 nm. These seminal studies exemplify the great potential of tuning phonon thermal conductivity via the phononic crystal effect, but were conducted only at cryogenic temperature so that the characteristic size of the artificial structures matches the wavelength of the phonons that dominate the thermal transport. As pointed out by Lee *et al.*, phonon coherence becomes negligible in silicon phononic crystals with a periodicity above 100 nm when the temperature is above 14 K [11], where incoherent phonon scatterings at the boundaries dominate the thermal transport [12]. Computationally, the hybridization of propagating long-wavelength acoustic phonons with local resonances introduced by artificial periodic structures has been shown to significantly alter the thermal conductivity, whereas the required size of the artificial structures is typically a few nanometers [13,14]. This small length scale indicates that, instead of artificial phononic crystals, a more promising route to observing and exploiting phononic crystal effects at a higher temperature is to examine thermal transport in natural materials with hierarchical superstructures matching the thermal phonon wavelength. Recently, Guo *et al.* used first-principles simulations to examine the phonon transport across van der Waals heterostructures with interlayer distances matching the thermal phonon wavelength, where they observed strong effects of phonon interference leading to highly anisotropic thermal conduction and ultralow thermal conductivity below the amorphous limit [15]. Due to the weak interlayer van der Waals interaction, however, the cross-plane thermal conductivity of van der Waals heterostructures is

*These authors contributed equally to this work.
†Corresponding author: bliao@ucsb.edu

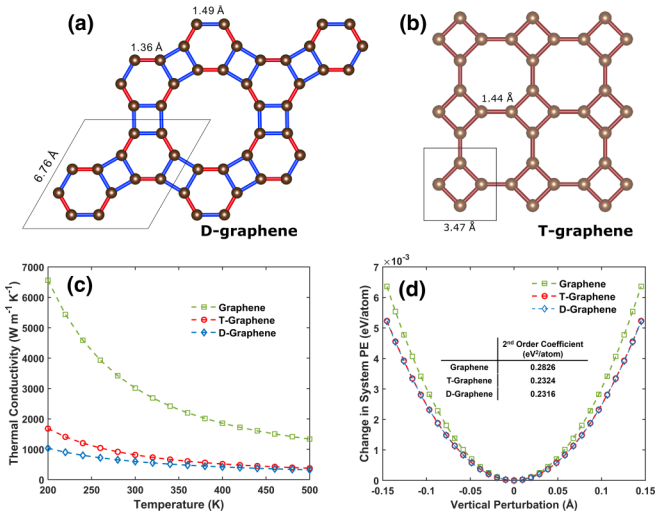

FIG. 1. Crystal structure and lattice parameters of (a) D-graphene and (b) T-graphene. (c) Calculated thermal conductivities of graphene, T-graphene, and D-graphene versus temperature. (d) Changes in total potential energy versus vertical perturbation of a carbon atom in graphene, T-graphene, and D-graphene, indicating the bonding strengths in the three carbon allotropes. The quadratic coefficients of the curves are quantitative descriptors of the bonding strengths and are given in the inset table. PE: potential energy.

intrinsically low, which limits the achievable tuning range. In this work, we use first-principles simulations to investigate in-plane phonon transport in graphene-based two-dimensional (2D) materials with an intrinsic superstructure, a secondary periodicity that matches the thermal phonon wavelength at room temperature. "Phononic crystal" effect in 2D materials is of particular interest due to its potential coexistence and interplay with other features of phonon transport, such as hydrodynamic phonon transport [16–18], enhanced resonant bonding [19], and electron-phonon interaction [20]. The two structures studied are metastable allotropes of graphene [21], named dodecagraphene (D-graphene) and tetragraphene (T-graphene) [22], as shown in Figs. 1(a) and 1(b). We observe a drastic reduction, up to 80% and 73%, of the intrinsic in-plane thermal conductivities of D-graphene and T-graphene compared to pristine graphene at room temperature despite similar bonding strengths, as shown in Fig. 1(c), which we attribute to the reduction of the phonon group velocity due to Brillouin zone folding induced by the superstructures, enhancement of the phonon scatterings and suppression of hydrodynamic phonon transport. Our analysis provides quantitative understanding about the impact of the periodic superstructure on various aspects of thermal transport in 2D materials and demonstrates the possibility of tailoring thermal conductivity of 2D materials without altering their fundamental compositions.

II. COMPUTATIONAL METHODS

The D-graphene unit cell contains 12 carbon atoms and is constructed by adjoining two graphene unit cells such that they do not share a side. The T-graphene has a square lattice with four carbon atoms in each unit cell. The crystal structures are shown in Figs. 1(a) and 1(b). Initial lattice parameters for D-graphene and T-graphene were taken from a previous study by Enyashin *et al.* [21], who reported a lattice constant of 6.83 Å and an average C-C distance of 1.449 Å for D-graphene and a lattice constant of 3.47 Å for T-graphene. The structures were constructed using these parameters and subsequently relaxed using density functional theory with the projector augmented wave method as implemented in the Vienna *ab initio* Simulation Package (VASP) [23,24]. Calculations were performed using the Perdew-Burke-Ernzerhof generalized gradient approximation exchange-correlation functionals. A $10 \times 10 \times 1$ Monkhorst-Pack k mesh was used to sample the graphene, D-graphene, and T-graphene Brillouin zones (BZs). A large vacuum space of 20 Å was introduced to minimize out-of-plane interactions that may have occurred through the use of periodic boundary conditions. All atomic positions were unconstrained and allowed to change until the maximum Hellman-Feynman forces were smaller than 0.01eV/Å per ion.

After relaxation, the initial C-C bonds in D-graphene degenerate into two distinct C-C bonds with lengths of 1.36 and 1.47 Å, and the lattice constant shrinks to 6.76 Å. The intergraphene bonds are each 1.47 Å in length, with each alternating bond being 1.36 Å. The C-C bonds in T-graphene relax into identical bonds 1.44 Å long. The structures, shown in Figs. 1(a) and 1(b), are metastable, with their total energy per atom being greater than that of pristine graphene, but existing in local energy minima.

To calculate the phonon dispersions of D-graphene and T-graphene, the second-order harmonic interatomic force constants (IFCs) were obtained by utilizing density functional perturbation theory [25] using the VASP package. Phonon dispersions for graphene, D-graphene, and T-graphene were calculated using these harmonic IFCs in concert with the PHONOPY package [26], and are shown in Fig. 2. Both D-graphene and T-graphene are dynamically stable as no imaginary frequencies are observed in their phonon dispersions.

The phonon Boltzmann transport equation (BTE) was solved using the ShengBTE [27] package in order to study the thermal transport properties of D-graphene and T-graphene. The lattice thermal conductivity tensor (κ) can be written

$$\kappa = \frac{1}{3} \sum_{p} \sum_{q} c_{\mathrm{ph}} v_g(p,q)^2 \tau(p,q),$$

where p and q are the phonon branch and wave vector, respectively, c_{ph} is the phonon specific heat capacity, $v_g = d\omega/dq$ is the phonon group velocity, and τ is the phonon lifetime and is also equivalent to the inverse of the phonon scattering rate. The calculation of κ required the calculation of the third-order, anharmonic IFCs, for which a $2 \times 2 \times 1$ D-graphene supercell and a $4 \times 3 \times 1$ T-graphene supercell was constructed, and the anharmonic IFCs were calculated using the finite-displacement method [28,29]. The D-graphene supercell contains 48 atoms and reveals a secondary symmetry, where six graphene unit cells adjoined by 1.47 Å bonds form a 12-sided carbon ring 5.27 Å in diameter. Due to the low density of atoms at the unit cell corners, these superstructures result in highly porous structures, a design archetype that is commonly found in many

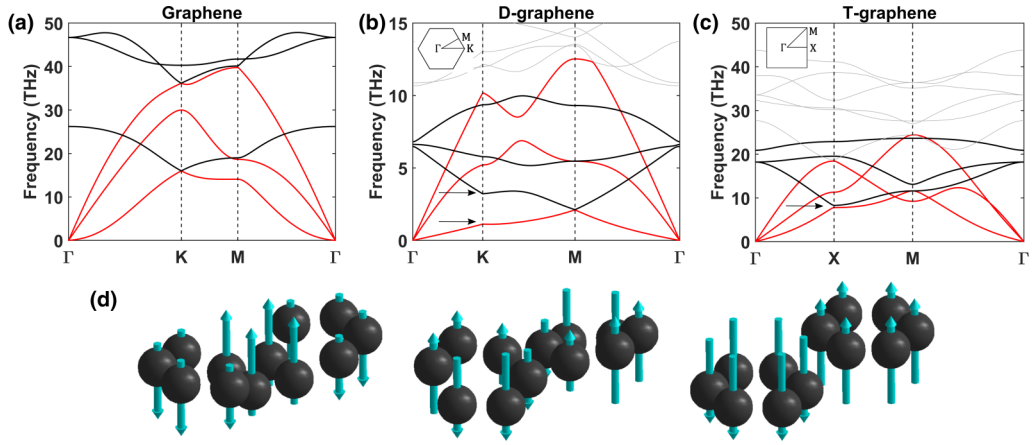

FIG. 2. Calculated phonon dispersion relations for (a) graphene, (b) D-graphene, and (c) T-graphene. The arrows in (b) and (c) indicate the frequency gaps opened due to zone folding and phonon interference. (d) Vibrational modes of the three low lying optical phonons in D-graphene, indicating their origins as collective motions of base units.

engineered thermal metamaterials [11,12,30,31], but with a much smaller characteristic length scale. Given the third-order anharmonic IFCs, the phonon BTE was solved iteratively using ShengBTE. A $30 \times 30 \times 1$ grid was used for D-graphene, whereas a $40 \times 40 \times 1$ grid was used for T-graphene. The convergence of the calculated thermal conductivities with the sampling mesh density was carefully checked and confirmed. The thickness of D- and T-graphene was taken as 3.4 Å, the same as monolayer graphene, for a fair comparison of their thermal conductivities. Due to the long mean free paths of the out-of-plane acoustic (ZA) phonons, the thermal conductivity of graphene diverges with increasing sample size even in the micrometer scale, as observed in experiments [32] and explained by simulation [33,34]. This is caused by the slow decay of boundary scattering rates of the long-mean-free-path acoustic phonons. In this work, since our purpose is to compare the intrinsic phonon thermal conductivity of graphene with those of D-graphene and T-graphene, we consider infinite sheets and do not include the phonon-boundary scattering effect.

III. RESULTS AND DISCUSSIONS

The calculated lattice thermal conductivities of graphene, D-graphene and T-graphene are shown in Fig. 1(c). While the room temperature thermal conductivity of graphene is ~3000 W/mK, in good agreement with established literature [35], the room temperature thermal conductivities of D-graphene and T-graphene are ~600 and ~800 W/mK, 80% and 73% reduction from that of graphene, respectively. All thermal conductivities exhibit the expected 1/T trend and the discrepancy in thermal conductivity is greatly exacerbated at lower temperatures. This large reduction of thermal conductivity is unexpected. First, the number density of carbon atoms in graphene, D-graphene and T-graphene are 0.383, 0.303, and 0.332 $Å^{-2}$, respectively. A first-order estimation using the effective medium theory [36], which considers the increased porosity of D-graphene and T-graphene but not the phonon-boundary scattering and zone-folding effects, would predict a thermal conductivity reduction of only 28% for D-graphene and 18% for T-graphene. Second, we examined the out-of-plane bonding strengths of the three carbon allotropes, which are responsible for the "stiffness" of the materials and the group velocity of the out-of-plane flexural phonons. Since the flexural phonons are major heat carriers in the three materials [35], their group velocity will have a strong influence on the thermal conductivity. The bonding strengths were quantified by calculating the change of the total potential energy of the allotropes when a carbon atom is displaced vertically (out-of-plane) from its equilibrium position. The quadratic coefficients of the energy change versus atomic displacement curves, as shown in Fig. 1(d), reflect the bonding strengths, whose numerical values are given in the inset table. The results indicate that D-graphene and T-graphene have similar out-of-plane bonding strengths, which are ~18% lower than that of graphene. As the acoustic phonon group velocity scales with the square root of the bonding strength (or the "spring constant"), this moderate reduction of the bonding strength still cannot explain the observed large difference in thermal conductivity between graphene and D- and T-graphene.

We hypothesize that the significant thermal conductivity reduction of D- and T-graphene is due to the phononic crystal effect, given that both structures contain a secondary periodicity compared to graphene. The D-graphene structure can be constructed by replacing each atom in a graphene honeycomb lattice with a hexagonal ring of carbon atoms. Similarly, the T-graphene structure can be constructed by combining a square lattice with a four-atom square basis. Imagine that if we want to periodically pattern graphene to make a phononic crystal, with an as-small-as-possible periodicity, the D-graphene structure is what we will obtain. Similarly we can think of T-graphene as a square lattice of carbon atoms with periodically patterned holes. As the periodicity of these superstructures (6.76 Å for D-graphene and 3.47 Å for T-graphene) is on the same order of the wavelength of the heat carrying acoustic phonons, it is expected that the phonons with matching wavelengths will be largely affected by the secondary periodicity and the phonon group velocity will be suppressed, as has been observed in artificial phononic crystals [4]. In

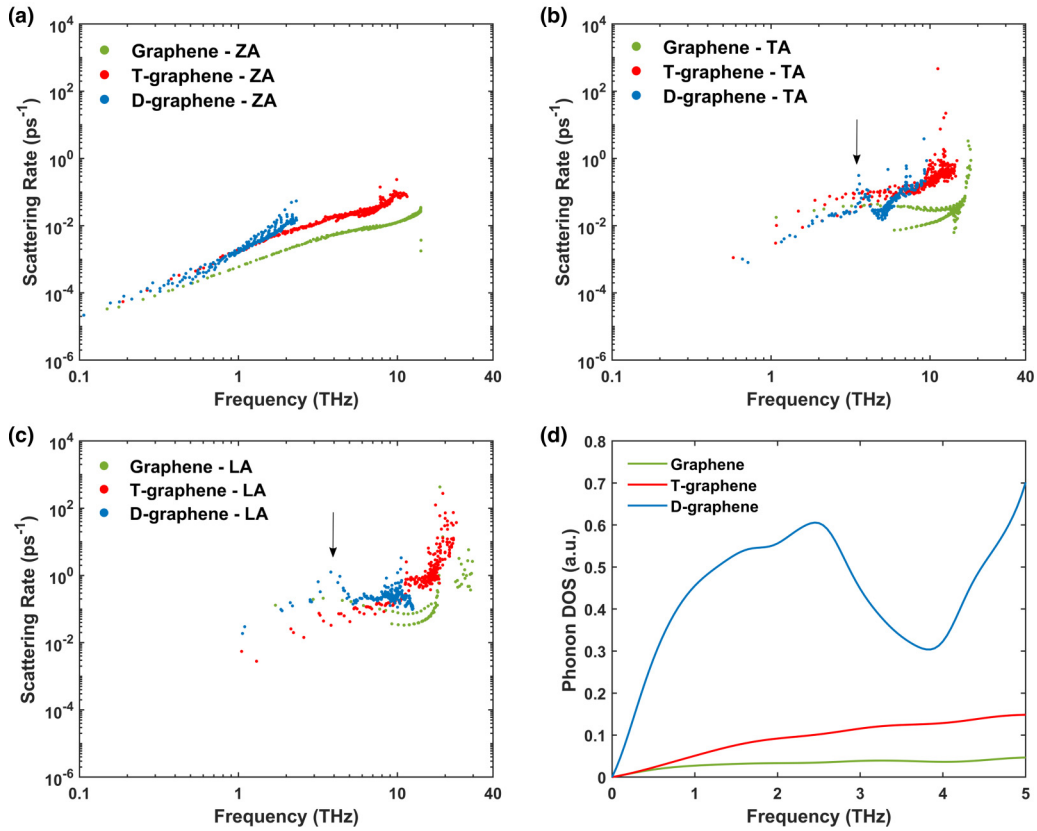

FIG. 3. Calculated phonon-phonon scattering rates of (a) ZA branches, (b) TA branches, and (c) LA branches in graphene, T-graphene, and D-graphene. The arrows in (b) and (c) indicate the peaks in the scattering rates for TA and LA branches in D-graphene due to the frequency gap of the ZA branch. (d) Phonon density of states of the three allotropes versus phonon frequency (0 to 5 THz).

the current case, however, these effects are expected to have appreciable effects on the thermal conductivity even at room temperature due to the much smaller characteristic lengths.

To verity our hypothesis, we first analyze the phonon dispersions of the three allotropes, as shown in Figs. 2(a)–2(c). We note here that the dispersion relations of the ZA phonons of D-graphene and T-graphene are not purely quadratic, as should be expected for 2D materials. The linear component present in the ZA phonon dispersion of 2D materials is a known problem in *ab initio* phonon calculations [37,38], due to the difficulty to numerically impose all symmetry invariances on the calculated interatomic force constants in a precise way. This problem is systematically analyzed by Carrete *et al.* [39], and seems to be associated with most currently available phonon simulation software packages. We did a numerical fitting of our calculated phonon dispersions of D-graphene and T-graphene and the linear component is present but small near the zone center. The major effect of the nonparabolic dispersion near the zone center, as discussed by Carrete *et al.* [39], is the difference in phonon density of states, which in turn affects the phonon scattering rates, but is only appreciable when the ZA phonon group velocity is high (such as in graphene and borophene). In our case, the D-graphene and T-graphene ZA phonon group velocity is much lower than graphene, and thus we do not expect any appreciable effect. Interestingly, the D-graphene and T-graphene dispersions show some markedly different behaviors from that of graphene. The maximum acoustic mode frequency in graphene is found in the longitudinal acoustic (LA) mode, and is ∼40 THz. This is significantly depressed in D-graphene and T-graphene, with a maximum frequency of ∼12.5 and ∼18 THz, respectively, due to band folding. Furthermore, the zone-boundary phonons open up partial frequency gaps in the dispersions in D-graphene and T-graphene. In the case of D-graphene, a frequency gap from ∼1 to ∼3 THz in the ZA branch is opened at the *K* point. In the case of T-graphene, a frequency gap around 8 THz in the ZA branch is opened at the *X* point. Although these are partial frequency gaps that do not cover the full BZ, they significantly suppress the group velocity of the ZA phonons and boost the phonon scatterings due to the flattened ZA dispersion and the increased ZA phonon density of states, as will be discussed later in detail.

Another interesting phenomenon is the occurrence of three low-lying optical (LLO) phonon modes in D-graphene that cross and interact heavily with the acoustic modes. Branch 4, the lowest lying optical mode and referred to as the ZO mode, couples heavily with the ZA mode along the BZ boundary. Branch 5 interacts strongly with the transverse acoustic (TA) mode. Branch 5 and the LA mode are coupled heavily along the *M*-*K* path. Branch 6 exhibits four distinct crossing events with the LA mode in the irreducible wedge. These LLO modes arise from the folding of the acoustic modes, which can be clearly seen along the Γ-*M* path. This effect is most clearly seen in the ZA and TA branches, with the associated folded acoustic modes being modes 4 and 5, respectively. Physically, the LLO phonons in D-graphene represent the

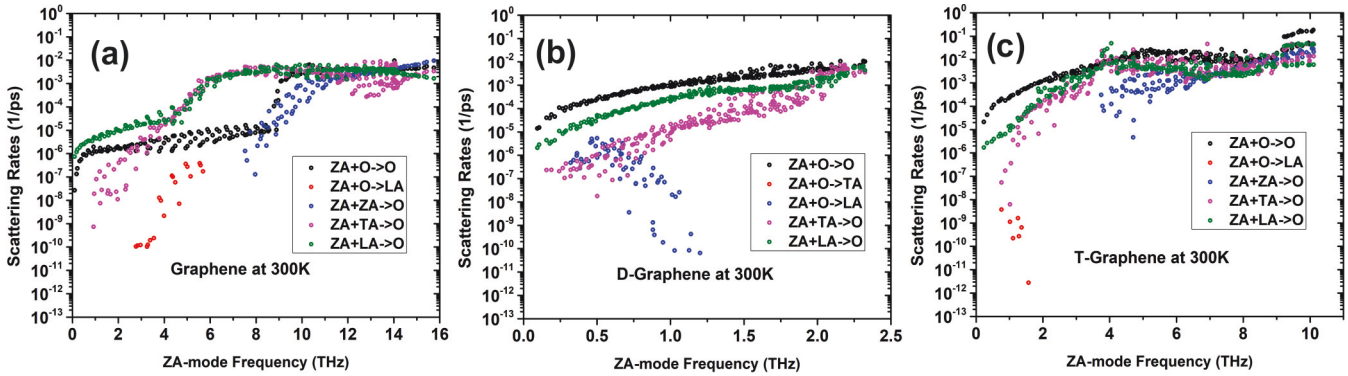

FIG. 4. Contributions from selected scattering channels to the total scattering rates of ZA phonons in (a) graphene, (b) D-graphene, and (c) T-graphene at 300 K.

collective motions of the six carbon atoms in hexagonal ring units, or "meta-atoms". As shown in Fig. 2(d), the ZO branch represents the bending of the unit cell about its center, with atoms at the edge of the unit cell being translated upwards out-of-plane, whereas an equal and opposite translation occurs in atoms near the unit cell center. Branch 5 resembles the twisting of the unit cell. Branch 6 represents whole-scale, out of phase, out-of-plane translations of the individual graphene unit cells. These LLO phonons are unique signatures originated from the secondary periodicity of D-graphene and are expected to strongly scatter the acoustic phonons and further suppress the thermal conductivity of D-graphene.

We further examine the phonon-phonon scattering rates of the acoustic modes in the three carbon allotropes, as shown in Fig. 3. The scattering rates of the ZA modes, shown in Fig. 3(a), in all three allotropes show similar scaling with the phonon frequency. The scattering rates in D-graphene and T-graphene are higher than those in graphene, mainly due to the increased phonon density of states in this frequency region, as shown in Fig. 3(d), which in turn is caused by the suppressed group velocity of the acoustic phonons in D-graphene and T-graphene. Of particular interest is the enhancement of phonon scattering near the frequency gaps, which is expected to happen due to the local high phonon density of states and enlarged phonon scattering phase space. This effect is clearly exhibited in the scattering rates of TA and LA phonons, as shown in Figs. 3(b) and 3(c). Clear peaks of scattering rates of both TA and LA phonons in D-graphene appear near 3 THz, which coincides with the upper edge of the frequency gap in D-graphene, as marked by the arrows in Figs. 3(b) and 3(c). In the case of T-graphene, upturns of the scattering rates for both TA and LA phonons are observed near 10 THz, as a result of strong hybridization between the ZA mode and the low-lying optical mode. These distinct features will significantly contribute to the reduction of the thermal conductivity of D-graphene and T-graphene.

As ZA phonons are the major heat carriers in graphene [35], we are particularly interested in the change of ZA phonon scattering in D-graphene and T-graphene as compared to that in graphene. For this purpose, we decompose the total ZA phonon scattering rates into contributions from different scattering channels, as shown in Fig. 4. It can be seen that the major enhancement of ZA phonon scattering is from the ZA + O $\rightarrow$ O channel, where one ZA phonon scatters with one optical phonon and produces another optical phonon. The scattering rate from this scattering channel is enhanced by two orders of magnitude for the low frequency portion of the ZA branch in D-graphene and T-graphene as compared to graphene. This is caused by zone folding and the presence of low-lying optical phonon modes in D-graphene and T-graphene, which will cause further reduction of the lattice thermal conductivity of D-graphene and T-graphene.

In Table I, we analyze the mode-specific contributions to the thermal conductivity. Acoustic modes contribute to almost the entirety of the conductivity of graphene and the ZA contribution comprises the majority of the conductivity, contributing 83.85%, which agrees with values previously reported [35]. The ZA contribution in D-graphene and T-graphene is reduced significantly, falling to roughly 47% and 60%, respectively, due to zone-folding and the reduced number of ZA phonon modes. In addition to the factors discussed previously, namely the reduced group velocity and enhanced scattering rates, another important factor is the breakdown of the hydrodynamic transport of the ZA phonons in D-graphene and T-graphene [16,18]. In graphene, the quadratic dispersion and strong anharmonicity of the ZA phonons lead to dominant momentum-conserving normal phonon-phonon scattering over the momentum-destroying Umklapp phonon-phonon scattering, which gives rise to hydrodynamic transport of the ZA phonons [16]. In the hydrodynamic regime, the phonon transport is much less dissipative, an effect that significantly contributes to the extraordinary high thermal conductivity of graphene. In D-graphene and T-graphene, however, the hydrodynamic transport of ZA phonons is expected to be suppressed, due to the shrunk Brillouin zone and the flattened ZA phonon dispersions. We verify this hypothesis by explicitly calculating the normal and Umklapp

TABLE I. Mode-specific contribution to the thermal conductivity in three carbon allotropes.

	Acoustic contribution	Optical contribution	ZA contribution
Graphene	97.14%	2.86%	83.85%
T-graphene	90.62%	9.38%	60.17%
D-graphene	81.85%	18.15%	46.83%

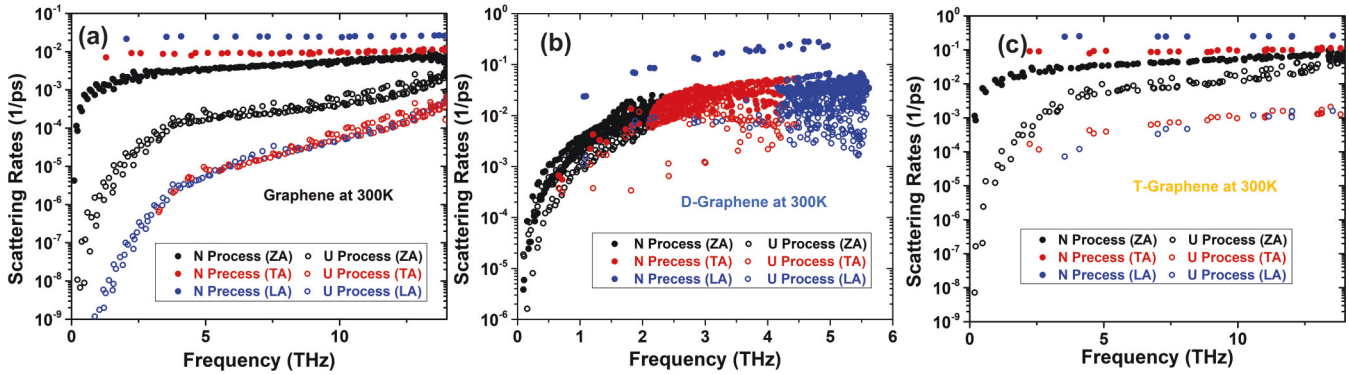

FIG. 5. Calculated phonon-phonon normal and Umklapp scattering rates of the three carbon allotropes at 300 K (a)–(c), indicating that hydrodynamic phonon transport in graphene is significantly suppressed in D-graphene due to comparable levels of normal and Umklapp scatterings and less affected in T-graphene.

phonon-phonon scattering rates in all three carbon allotropes at 300 K, as displayed in Fig. 5. In the case of graphene [Fig. 5(a)], the normal phonon scattering rates are one to two orders of magnitude higher than the Umklapp phonon scattering rates. In the case of D-graphene [Fig. 5(b)], however, the normal and Umklapp phonon scattering rates are at comparable levels at 300 K, especially for the low-frequency acoustic phonons that are the major heat carriers in these materials. The breakdown of hydrodynamic phonon transport in D-graphene will significantly increase the dissipation during heat conduction and further suppress its thermal conductivity. In comparison, the hydrodynamic transport in T-graphene [Fig. 5(c)] is less affected than that in D-graphene, possibly due to the larger Brillouin zone and more dispersed acoustic modes.

In summary, we apply first-principles phonon simulation to understand the thermal transport of carbon allotropes D-graphene and T-graphene with a secondary periodicity compared to graphene. Although D-graphene and T-graphene are 2D carbon materials constructed out of graphene unit cells and similar carbon-carbon bonds, and thus possess a fundamental composition favorable to efficient thermal transport, we find the thermal conductivities of D-graphene and T-graphene are significantly reduced from that of graphene. The introduction of a secondary in-plane periodicity results in the folding of the acoustic mode dispersions in D-graphene and T-graphene, creating frequency gaps at the Brillouin zone boundaries due to phonon interference. This effect leads to suppressed ZA phonon group velocity, enhanced phonon scattering near the frequency gaps and the breakdown of hydrodynamic phonon transport, reducing the overall lattice thermal conductivity. The four to five times reduction in thermal conductivity is attributed almost entirely to the introduction of the secondary periodicity of the superstructure, as the main structure inherent to graphene and the carbon-carbon bond strengths have largely been maintained. Our study presents D-graphene and T-graphene as ideal platforms to explore the phononic crystal effect on thermal conductivity at practical temperatures and provides quantitative insights about manipulating heat conduction utilizing the concept of phononic crystals, although significant experimental efforts will be required to verify our findings given the large difference in formation energies between graphene and D-graphene (0.8 eV/atom) and T-graphene (2.1 eV/atom) [21].

ACKNOWLEDGMENTS

This work is based on research supported by the US Department of Energy, Office of Basic Energy Sciences, Division of Materials Science and Engineering through the Early Career Research Program under the award number DE-SC0019244. B.L. acknowledges the support provided by the Regents' Junior Faculty Fellowship and an Academic Senate Faculty Research Grant from UCSB. We acknowledge computational resource support from the Center for Scientific Computing from the CNSI, MRL, a National Science Foundation (NSF) MRSEC (Grant No. DMR-1720256) and NSF Grant No. CNS-1725797. This work also used the Extreme Science and Engineering Discovery Environment (XSEDE) Stampede 2 at the Texas Advanced Computing Center (TACC) through allocation TG-DMR180044. XSEDE is supported by NSF Grant No. ACI-1548562.

[1] J. D. Joannopoulos, P. R. Villeneuve, and S. Fan, Nature (London) **386**, 143 (1997).
[2] N. Kaina, F. Lemoult, M. Fink, and G. Lerosey, Nature (London) **525**, 77 (2015).
[3] N. Fang, D. Xi, J. Xu, M. Ambati, W. Srituravanich, C. Sun, and X. Zhang, Nat. Mater. **5**, 452 (2006).
[4] M. Maldovan, Nature (London) **503**, 209 (2013).
[5] B. Liao and G. Chen, MRS Bull. **40**, 746 (2015).
[6] R. Anufriev, A. Ramiere, J. Maire, and M. Nomura, Nat. Commun. **8**, 15505 (2017).
[7] S. Alaie, D. F. Goettler, M. Su, Z. C. Leseman, C. M. Reinke, and I. El-Kady, Nat. Commun. **6**, 7228 (2015).
[8] M. N. Luckyanova, J. Garg, K. Esfarjani, A. Jandl, M. T. Bulsara, A. J. Schmidt, A. J. Minnich, S. Chen, M. S. Dresselhaus, Z. Ren, E. A. Fitzgerald, and G. Chen, Science **338**, 936 (2012).

[9] M. N. Luckyanova, J. Mendoza, H. Lu, B. Song, S. Huang, J. Zhou, M. Li, Y. Dong, H. Zhou, J. Garlow, L. Wu, B. J. Kirby, A. J. Grutter, A. A. Puretzky, Y. Zhu, M. S. Dresselhaus, A. Gossard, and G. Chen, Sci. Adv. **4**, eaat9460 (2018).

[10] J. Ravichandran, A. K. Yadav, R. Cheaito, P. B. Rossen, A. Soukiassian, S. J. Suresha, J. C. Duda, B. M. Foley, C.-H. Lee, Y. Zhu, A. W. Lichtenberger, J. E. Moore, D. A. Muller, D. G. Schlom, P. E. Hopkins, A. Majumdar, R. Ramesh, and M. A. Zurbuchen, Nat. Mater. **13**, 168 (2014).

[11] J. Lee, W. Lee, G. Wehmeyer, S. Dhuey, D. L. Olynick, S. Cabrini, C. Dames, J. J. Urban, and P. Yang, Nat. Commun. **8**, 14054 (2017).

[12] A. Vega-Flick, R. A. Duncan, J. K. Eliason, J. Cuffe, J. A. Johnson, J.-P. M. Peraud, L. Zeng, Z. Lu, A. A. Maznev, E. N. Wang, J. J. Alvarado-Gil, M. Sledzinska, C. M. Sotomayor Torres, G. Chen, and K. A. Nelson, AIP Adv. **6**, 121903 (2016).

[13] B. L. Davis and M. I. Hussein, Phys. Rev. Lett. **112**, 055505 (2014).

[14] S. Xiong, K. Sääskilahti, Y. A. Kosevich, H. Han, D. Donadio, and S. Volz, Phys. Rev. Lett. **117**, 025503 (2016).

[15] R. Guo, Y.-D. Jho, and A. J. Minnich, Nanoscale **10**, 14432 (2018).

[16] S. Lee, D. Broido, K. Esfarjani, and G. Chen, Nat. Commun. **6**, 6290 (2015).

[17] A. Cepellotti, G. Fugallo, L. Paulatto, M. Lazzeri, F. Mauri, and N. Marzari, Nat. Commun. **6**, 6400 (2015).

[18] R. Yang, S. Yue, and B. Liao, Nano. Micro. Thermophys. Eng. **23**, 25 (2019).

[19] S.-Y. Yue, T. Xu, and B. Liao, Mater. Today Phys. **7**, 89 (2018).

[20] B. Liao, J. Zhou, B. Qiu, M. S. Dresselhaus, and G. Chen, Phys. Rev. B **91**, 235419 (2015).

[21] A. N. Enyashin and A. L. Ivanovskii, Phys. Status Solidi B **248**, 1879 (2011).

[22] Y. Liu, G. Wang, Q. Huang, L. Guo, and X. Chen, Phys. Rev. Lett. **108**, 225505 (2012).

[23] G. Kresse and J. Furthmüller, Comput. Mater. Sci. **6**, 15 (1996).

[24] G. Kresse and J. Furthmüller, Phys. Rev. B **54**, 11169 (1996).

[25] S. Baroni, S. de Gironcoli, A. Dal Corso, and P. Giannozzi, Rev. Mod. Phys. **73**, 515 (2001).

[26] A. Togo, F. Oba, and I. Tanaka, Phys. Rev. B **78**, 134106 (2008).

[27] W. Li, J. Carrete, N. A. Katcho, and N. Mingo, Comp. Phys. Commun. **185**, 1747 (2014).

[28] D. A. Broido, M. Malorny, G. Birner, N. Mingo, and D. A. Stewart, Appl. Phys. Lett. **91**, 231922 (2007).

[29] K. Esfarjani, G. Chen, and H. T. Stokes, Phys. Rev. B **84**, 085204 (2011).

[30] J. Maire, R. Anufriev, R. Yanagisawa, A. Ramiere, S. Volz, and M. Nomura, Sci. Adv. **3**, e1700027 (2017).

[31] N. Zen, T. A. Puurtinen, T. J. Isotalo, S. Chaudhuri, and I. J. Maasilta, Nat. Commun. **5**, 3435 (2014).

[32] X. Xu, L. F. C. Pereira, Y. Wang, J. Wu, K. Zhang, X. Zhao, S. Bae, C. Tinh Bui, R. Xie, J. T. L. Thong, B. H. Hong, K. P. Loh, D. Donadio, B. Li, and B. Özyilmaz, Nat. Commun. **5**, 3689 (2014).

[33] L. Lindsay, W. Li, J. Carrete, N. Mingo, D. A. Broido, and T. L. Reinecke, Phys. Rev. B **89**, 155426 (2014).

[34] A. K. Majee and Z. Aksamija, Phys. Rev. B **93**, 235423 (2016).

[35] L. Lindsay, D. A. Broido, and N. Mingo, Phys. Rev. B **82**, 115427 (2010).

[36] C.-W. Nan, R. Birringer, D. R. Clarke, and H. Gleiter, J. Appl. Phys. **81**, 6692 (1997).

[37] H. Xie, M. Hu, and H. Bao, Appl. Phys. Lett. **104**, 131906 (2014).

[38] A. Jain and A. J. H. McGaughey, Sci. Rep. **5**, 8501 (2015).

[39] J. Carrete, W. Li, L. Lindsay, D. A. Broido, L. J. Gallego, and N. Mingo, Mater. Res. Lett. **4**, 204 (2016).